Causal differencing in ADM and conformal ADM formulations: A comparison in spherical symmetry

Luis Lehner,[1] Mijan Huq,[2] and David Garrison[3]
[1]*Center for Relativity, The University of Texas at Austin, Austin, Texas 78712*
[2]*Department of Astronomy & Astrophysics, The Pennsylvania State University, University Park, Pennsylvania 16802*
[3]*Center for Gravitational Physics & Geometry, The Pennsylvania State University, University Park, Pennsylvania 16802*
(Received 12 May 2000; published 22 September 2000)

Black hole excision is at present the most promising approach to deal with the singularities in black hole spacetimes. The implementation of this technique is done through carefully designed algorithms that exploit the causal structure of the spacetime in the black hole region. Causal differencing has shown to be one of the promising algorithms. To date, it has only been actively implemented in the Arnowitt-Deser-Misner (ADM) and Einstein-Bianchi 3+1 formulations of the Einstein equations. Recently, an approach closely related to the ADM one, commonly referred to as ''conformal ADM'' (CADM) method has shown excellent results when modeling waves on flat spacetimes and black hole spacetimes where singularity avoiding slices are used to deal with the singularity. In these cases, the use of the CADM method has yielded longer evolutions and better outer boundary dependence than those obtained with the ADM one. If this success translates to the case where excision is implemented, then the CADM formulation will likely be a prime candidate for modeling generic black hole spacetimes. In the present work we investigate the applicability of causal differencing to the CADM method, presenting the equations in a convenient way for such a task. We investigate whether the causal differencing implementation already developed for the ADM system can be extended to the CADM one.

PACS number(s): 04.25.Dm, 04.30.Db

I. INTRODUCTION

One of the goals of numerical relativity that has proven to be elusive (using a 3+1 splitting of the Einstein equations) has been that of modeling a generic single black hole for long periods of time. Present single black hole simulations in 3D have not yet been shown to be generically stable. There are limited instances of stability based on the outer boundary choice and placement [1,2]. Most simulations run just beyond a few hundreds M based on outer boundary placement and binary black hole simulations run for about $20-50M$ before the codes either crash or the entire grid is inside the event horizon. In some cases, the reason of the crash is well understood. For instance, the use of singularity avoiding slices leads to the presence of steep gradients which eventually can no longer be handled by the codes. A solution to this problem is to ''excise'' the singularity from the computational domain [3]. Unfortunately, in most cases, it is not clear what the main reasons behind the crash are and consequently addressing the problem becomes cumbersome. In attempting to deal with this issue there are several possible avenues to either remove or provide an understanding of the source of problems. These avenues can be divided in the following way: (1) choice of formulation of Einstein equations; (2) choice of gauge; (3) numerical implementations. Avenue (1) is motivated by the difficulties encountered in achieving long term evolutions with the Arnowitt-Deser-Misner (ADM) formulation, which historically has been the main tool in numerical relativity. Several formulations exist in the literature that exhibit properties such as hyperbolicity [4], the equations are expressed in a flux conservative form [5] and/or try to separate transverse modes [6–8]. Avenue (2) is based on the fact that, in principle, a coordinate system could be chosen such that the fields vary slowly in time; hence, the simulations would be better behaved. Conditions to achieve such coordinates have been presented in the literature [9]. Lastly, avenue (3) highlights the need for a more profound understanding of the numerical implementation of the evolution equations. Algorithms specifically tailored to deal with the equations under study could pave the way to better behaved simulations (for instance, compare with the implementations that deal with the fluid equations and their ''historical evolution'' from crude implementations in early simulations to high resolution shock capturing schemes in present state of the art codes [10]).

Our present work focuses primarily on avenue (1); although avenues (2) and (3) also play a role since notable improvements are achieved with specific gauge choices and the use of causal differencing algorithms. We compare results obtained from the use of black hole excision via causal differencing in the standard ADM and conformal ADM (CADM) system of equations in spherical symmetry (1D).

The main motivation behind the comparison with the conformal ADM is the report by many groups that robust implementations have been achieved in linearized gravity, gravitational wave spacetimes, systems containing matter, etc. [11,7,12]. However, so far, it has only been used to model black hole spacetimes using singularity avoiding slices [13]. As it is widely accepted, these types of slicings are useful when the desired simulation time is rather short. In order to model black hole spacetimes for long periods of time, singularity excision must be employed. To study the feasibility of excision through *causal differencing* in this formulation and to analyze its advantages and disadvantages with respect to the traditional ADM formulation (where causal differencing has been used for several years already [14,15]), we present a 1D study and compare results obtained with both ap-

proaches. We start with a brief review of the formulations in Sec. II. In Sec. III, we rewrite the system of equations in a way convenient for causal differencing and describe how this technique is implemented. In Sec. IV we compare simulations of a Schwarzschild black hole and show how the ADM formulation yields longer term evolution *unless* the trace of the extrinsic curvature is frozen in time, in which case CADM yields better behaved evolutions than the ADM formulation, we also show how causal differencing indeed gives the expected results in terms of stability. We conclude in Sec. V with a brief discussion and include in the Appendix a study of how a choice of interpolating stencils can indeed affect the overall stability of an evolution algorithm.

II. FORMULATION

The standard ADM equations corresponding to the vacuum case, in the form most commonly used in numerical relativity, are [16]

$$\frac{d}{dt}\gamma_{ij} = -2\alpha K_{ij}, \tag{2.1a}$$

$$\frac{d}{dt}K_{ij} = -D_i D_j \alpha + \alpha(R_{ij} + K K_{ij} - 2K_{ik}K^k{}_j), \tag{2.1b}$$

with

$$\frac{d}{dt} = \partial_t - \mathcal{L}_\beta, \tag{2.2}$$

where $\mathcal{L}_\beta$ is the Lie derivative along the shift vector β^i; R_{ij} is the Ricci tensor and D_i the covariant derivative associated with the three-dimensional metric γ_{ij}.

The conformal ADM equations [6,7] are obtained from the ADM ones by (I) making use of a conformal decomposition of the three-metric as

$$\tilde{\gamma}_{ij} = e^{-4\phi}\gamma_{ij} \quad \text{with} \quad e^{4\phi} = \gamma^{1/3} \equiv \det(\gamma_{ij})^{1/3} \tag{2.3}$$

[hence $\det(\tilde{\gamma}) = 1$]. (II) Decomposing the extrinsic curvature into its trace and trace-free components. The trace-free part of the extrinsic curvature K_{ij}, defined by

$$A_{ij} = K_{ij} - \frac{1}{3}\gamma_{ij}K, \tag{2.4}$$

and $K = \gamma^{ij}K_{ij}$ is the trace of the extrinsic curvature. (III) Further conformally decomposing A_{ij} as

$$\tilde{A}_{ij} = e^{-4\phi}A_{ij}. \tag{2.5}$$

In terms of these variables, Einstein equations in vacuum are [6,7]

$$\frac{d}{dt}\tilde{\gamma}_{ij} = -2\alpha\tilde{A}_{ij}, \tag{2.6a}$$

$$\frac{d}{dt}\phi = -\frac{1}{6}\alpha K, \tag{2.6b}$$

$$\frac{d}{dt}K = -\gamma^{ij}D_i D_j\alpha + \alpha\left(\tilde{A}_{ij}\tilde{A}^{ij} + \frac{1}{3}K^2\right), \tag{2.6c}$$

$$\frac{d}{dt}\tilde{A}_{ij} = e^{-4\phi}[-D_i D_j\alpha + \alpha R_{ij}]^{TF} + \alpha(K\tilde{A}_{ij} - 2\tilde{A}_{il}\tilde{A}^l_j), \tag{2.6d}$$

where the Hamiltonian constraint was used to eliminate the Ricci scalar in equation (2.6c). Note that with the conformal decomposition of the three-metric, the Ricci tensor now has two pieces, which are written as

$$R_{ij} = \tilde{R}_{ij} + R^\phi_{ij}. \tag{2.7}$$

The ''conformal-factor'' part R^ϕ_{ij} is given directly by straightforward computation of derivatives of ϕ:

$$R^\phi_{ij} = -2\tilde{D}_i\tilde{D}_j\phi - 2\tilde{\gamma}_{ij}\tilde{D}^l\tilde{D}_l\phi \tag{2.8}$$

$$+4\tilde{D}_i\phi\tilde{D}_j\phi - 4\tilde{\gamma}_{ij}\tilde{D}^l\phi\tilde{D}_l\phi, \tag{2.9}$$

while the ''conformal'' part $\tilde{R}_{ij}$ can be computed in the standard way from the conformal three-metric $\tilde{\gamma}_{ij}$.

To this point, the equations have been written by a trivial algebraic manipulation of the ADM equations in terms of the new variables. The non-trivial part comes into play by introducing what Ref. [7] calls the ''conformal connection functions''

$$\tilde{\Gamma}^i := \tilde{\gamma}^{jk}\tilde{\Gamma}^i_{jk} = -\tilde{\gamma}^{ij}{}_{,j}, \tag{2.10}$$

where the last equality holds since the determinant of the conformal three-metric $\tilde{\gamma}$ is unity. Using the conformal connection functions, the Ricci tensor is written as

$$\tilde{R}_{ij} = -\frac{1}{2}\tilde{\gamma}^{lm}\tilde{\gamma}_{ij,lm} + \tilde{\gamma}_{k(i}\partial_{j)}\tilde{\Gamma}^k + \tilde{\Gamma}^k\tilde{\partial}_{(j}\tilde{\gamma}_{i)k}$$

$$-\tilde{\gamma}^{kl}_{(,j}\tilde{\gamma}_{i)l,k} - \tilde{\Gamma}^l\tilde{\Gamma}_{ijl} - \Gamma^l_{kj}\Gamma^k_{li}. \tag{2.11}$$

where $\tilde{\Gamma}^i$ are to be considered independent variables whose evolution equations are obtained by a simple commutation of derivatives

$$\frac{\partial}{\partial t}\tilde{\Gamma}^i = -\frac{\partial}{\partial x^j}\left(2\alpha\tilde{A}^{ij} - 2\tilde{\gamma}^{m(j}\beta^{i)}{}_{,m} + \frac{2}{3}\tilde{\gamma}^{ij}\beta^l{}_{,l} + \beta^l\tilde{\gamma}^{ij}{}_{,l}\right). \tag{2.12}$$

Finally, as shown in Refs. [7,17,12], it is crucial to replace the divergence of $\tilde{A}^{ij}$ with the help of the momentum constraint to obtain

$$\frac{\partial}{\partial t}\tilde{\Gamma}^i = -2\tilde{A}^{ij}\alpha_{,j} + 2\alpha\left(\tilde{\Gamma}^i_{jk}\tilde{A}^{kj} - \frac{2}{3}\tilde{\gamma}^{ij}K_{,j} + 6\tilde{A}^{ij}\phi_{,j}\right) + \beta^l\tilde{\Gamma}^i_{,l}$$

$$+\frac{1}{3}\tilde{\gamma}^{mi}\beta^j_{,mj} + \tilde{\gamma}^{mj}\beta^i_{,mj} - \tilde{\Gamma}^m\beta^i_{,m} + \frac{2}{3}\tilde{\Gamma}^i\beta^l_{,l}. \tag{2.13}$$

With this reformulation, in addition to the evolution equations for the conformal three-metric $\tilde{\gamma}_{ij}$ (2.6a) and the conformal-traceless extrinsic curvature variables $\tilde{A}_{ij}$ (2.6d), there are evolution equations for the conformal factor ϕ (2.6b), the trace of the extrinsic curvature K (2.6c) and the conformal connection functions $\tilde{\Gamma}^i$ (2.13).

III. CAUSAL DIFFERENCING IMPLEMENTATION

Causal differencing, as explained in Refs. [18–22], provides a straightforward way to integrate the evolution equations while preserving (and taking advantage of) the causal structure of the spacetime under consideration. In the approach used in the present work we follow the strategy described in Refs. [21,22]. First, the Lie derivative along β^i is split and terms containing derivatives of β^i are moved to the right hand side. Then, the ADM system of equations is reexpressed as

$$\partial_o \gamma_{ij} = -2\alpha\gamma_{ij} + 2\gamma_{l(i}\beta^l_{,j)}, \tag{3.1a}$$

$$\partial_o K_{ij} = D_i D_j \alpha + \alpha(R_{ij} + KK_{ij} - 2K_{ik}K^k{}_j - {}^{(4)}R_{ij}) + 2K_{l(i}\beta^l_{,j)} \tag{3.1b}$$

and the CADM system of equations then reduces to

$$\partial_o \tilde{\gamma}_{ij} = -2\alpha\tilde{A}_{ij} + 2\tilde{\gamma}_{l(i}\beta^l_{,j)}, \tag{3.2a}$$

$$\partial_o \phi = -\frac{1}{6}\alpha K + \frac{1}{6}\beta^i_{,i}, \tag{3.2b}$$

$$\partial_o K = -\gamma^{ij} D_i D_j \alpha + \alpha\left[\tilde{A}_{ij}\tilde{A}^{ij} + \frac{1}{3}K^2\right], \tag{3.2c}$$

$$\partial_o \tilde{A}_{ij} = e^{-4\phi}[-D_i D_j \alpha + \alpha R_{ij}]^{TF} + \alpha(K\tilde{A}_{ij} - 2\tilde{A}_{il}\tilde{A}^l_j) + 2\tilde{A}_{k(j}\beta^k_{,i)} - \frac{2}{3}\tilde{A}_{ij}\beta^k_{,k}, \tag{3.2d}$$

$$\partial_o \tilde{\Gamma}^i = -2\tilde{A}^{ij}\alpha_{,j} + 2\alpha\left(\tilde{\Gamma}^i_{jk}\tilde{A}^{kj} - \frac{2}{3}\tilde{\gamma}^{ij}K_{,j} + 6\tilde{A}^{ij}\phi_{,j}\right) + \frac{1}{3}\tilde{\gamma}^{mi}\beta^j_{,mj} + \tilde{\gamma}^{mj}\beta^i_{,mj} - \tilde{\Gamma}^m\beta^i_{,m} + \frac{2}{3}\tilde{\Gamma}^i\beta^l_{,l}, \tag{3.2e}$$

where $\partial_o \equiv \partial_t - \beta^i\partial_i$.

Finally the numerical implementation of the equations is split into two steps. First, the equations are evolved along the normal to the hypersurface (at constant t) $n^a = \partial^a_t - \beta^i\partial^a_i$. In the second step, an interpolation is carried over to obtain values on grid coordinate locations (see Fig. 1). Note that the two systems of equations have in this form the same basic structure; hence, simple modifications to an ADM code with excision (such as AGAVE [23]) will enable the use of already developed excision modules with the CADM equations in a straightforward manner.[1]

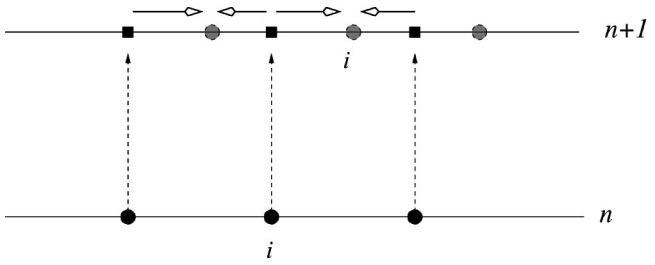

FIG. 1. Illustration of the causal differencing strategy. First the integration proceeds along the dashed lines to obtain values in the $n+1$ level (at filled square points). Then, an interpolation is carried out to obtain values on the grid points (filled circles). In the graph, as an example, a second order interpolation (indicated with arrows) provides values on the ith grid point.

Numerical implementation. A second order finite difference code has been written to implement both the ADM and CADM formulations.[2] We discretize the radial coordinate r as $r = r_{\min} + (i-1)\Delta r$ [for $i = 1, \ldots, N_r$ and $\Delta r = (r_{\max} - r_{\min})/(N_r - 1)$] and fix $\Delta t = \alpha\Delta r$ (with $\alpha = 1/4$). We discretize the equations by standard second order centered finite differences (except at the boundaries where sided second order accurate approximations are implemented in the standard way). As stated in the previous section, the integration is divided in two steps. The first one actually advances field values from level n to $n+1$ through the use of an ''iterative Crank Nicholson'' algorithm [24,12] (with two iterations) while the second one involves an interpolation for every grid point. Near an excision boundary the choice of interpolation order and stencil becomes important. We allow a choice of second, third and fourth order interpolations in order to study possible practical approaches. (The Appendix includes a stability analysis of these options.)

Finally, in the numerical implementation of the CADM it is convenient to introduce an intermediate variable F such that $\phi \equiv 1/4\ln(F)$ and evolve F instead of ϕ. This choice avoids unnecessary handling of exponential and logarithmic functions thus preventing loss of accuracy; hence, the equation for F is

$$\partial_o F = -\frac{2}{3}\alpha F K + \frac{2}{3}F\beta^i_{,i}. \tag{3.3}$$

IV. APPLICATIONS

To compare evolutions with the above formulations we pick as a particular example the Schwarzschild spacetime (and linear perturbations of it). In order to implement excision, a slicing must be chosen such that surfaces of constant

[1]These modifications are in place in the AGAVE code and currently being tested in 3D.

[2]This code is publicly available and can be requested from the authors.

time ''penetrate'' the horizon. The ingoing Eddington-Finkelstein coordinates [25] define hypersurfaces satisfying this condition; in terms of them, the line element reads

$$ds^2 = -\left(1-\frac{2M}{r}\right)dt^2 + \frac{4M}{r}dtdr + \left(1+\frac{2M}{r}\right)dr^2 + r^2 d\Omega^2, \tag{4.1}$$

where $d\Omega^2 = d\theta^2 + \sin^2\theta d\phi^2$. The lapse and shift vector are therefore

$$\alpha = \sqrt{\frac{r}{r+2M}}; \quad \beta^i = \frac{2M}{r+2M}\delta^i_r. \tag{4.2}$$

The basic ADM variables read

$$\begin{aligned} \gamma_{rr} &= 1+2\frac{M}{r}, \\ \gamma_{\theta\theta} &= r^2 = \frac{\gamma_{\phi\phi}}{\sin^2\theta}, \\ K_{rr} &= -\frac{2M}{r^3}(r+M)\alpha, \\ K_{\theta\theta} &= 2M\alpha = \frac{K_{\phi\phi}}{\sin^2\theta} \end{aligned} \tag{4.3}$$

and the CADM variables

$$\begin{aligned} \phi &= \frac{1}{4}\ln\{[(r+2M)r^3\sin^2\theta]^{1/3}\}, \\ K &= \frac{2M\alpha}{r^2}\frac{(r+3M)}{(r+2M)}, \\ \tilde{\gamma}_{rr} &= \frac{r+2M}{r^2[(r+2M)\sin^2\theta]^{1/3}}, \\ \tilde{\gamma}_{\theta\theta} &= \frac{r}{[(r+2M)\sin^2\theta]^{1/3}} = \frac{\tilde{\gamma}_{\phi\phi}}{\sin^2\theta}, \\ \tilde{A}_{rr} &= -\frac{4M}{3}\frac{\alpha(2r+3M)}{r^4[(r+2M)\sin^2\theta]^{1/3}}, \\ \tilde{A}_{\theta\theta} &= \frac{2M}{3}\frac{\alpha(2r+3M)}{r(r+2M)[(r+2M)\sin^2\theta]^{1/3}} = \frac{\tilde{A}_{\phi\phi}}{\sin^2\theta}, \\ \tilde{\Gamma}^r &= -\frac{4}{3}\frac{r^3(r+3M)\sin^2\theta}{r^2(r+2M)^{5/3}}, \\ \tilde{\Gamma}^\theta &= -\frac{2}{3}\frac{r(r+2M)\cos\theta}{r^2(r+2M)^{2/3}\sin^{2/3}\theta}, \\ \tilde{\Gamma}^\phi &= 0. \end{aligned} \tag{4.4}$$

Our slicing condition is thus provided by the analytical values of α and β [Eqs. (4.2)] and we choose to keep these fixed throughout the evolution unless otherwise specified.

Note that some of the quantities are functions of θ. In our spherically symmetric implementation of these equations we have explicitly expressed each variable as a function of r times the exact function of the angle θ. For instance, we write

$$\tilde{\gamma}_{\theta\theta} = h_{\theta\theta}(r)/\sin^2\theta. \tag{4.5}$$

Proceeding this way allows for the explicit appearance of θ to drop out of the equations, providing at the end of the day, a truly $1D$ system of equations corresponding to spherical symmetry.

A. Comparison

Extended tests were performed with both codes (under the same conditions) to understand the robustness of each formulation with excision. As has been observed in previous work [7,12], CADM gives long term evolutions when the evolution of K is ''frozen;'' i.e., the equation for K is not evolved or the value of K is fixed by the choice of a slicing that leaves K fixed (for instance, maximal slicing that fixes $K=0$.). On the other hand, longer term evolutions have also been achieved with an ''area locking gauge'' in the ADM formulation [26]. We then perform three basic tests.

Fully free evolution: All equations corresponding to each system are integrated without imposing any further condition.

''Locked'' evolution: Conditions on some of the field variables are enforced (see below).

''Perturbed'' evolution: Same as the ''locked'' case but considering linear perturbations of Schwarzschild spacetime as initial data.

In all these tests, we study the dependence of the obtained solution under discretization size and location of the outer boundary. The inner boundary is placed at $r=M$ and the outer boundary is varied (placed at $r=nM$) while keeping $\Delta r = \text{const}$. Outer boundary data are provided by ''blending'' [27] the numerical solution to the analytical one. This choice reduces gradients and second derivatives at the boundary allowing for a clean evolution without much reflection from the outer boundary.

1. Fully free evolution

In this case, all equations corresponding to systems (3.1),(3.2) are evolved and the obtained solutions are compared. We use the Hamiltonian and momentum constraint as monitors of the quality of the evolution. Our results can be summarized as follows. For the ADM formulation we observed that stable evolutions are obtained if $n \lesssim 6$ while for larger $n \gtrsim 6$ the solution exhibits exponentially growing modes. It is worth emphasizing that the evolution is not unstable in the strict sense (i.e., the solution can be bounded from above by an exponential [28].). However, the presence

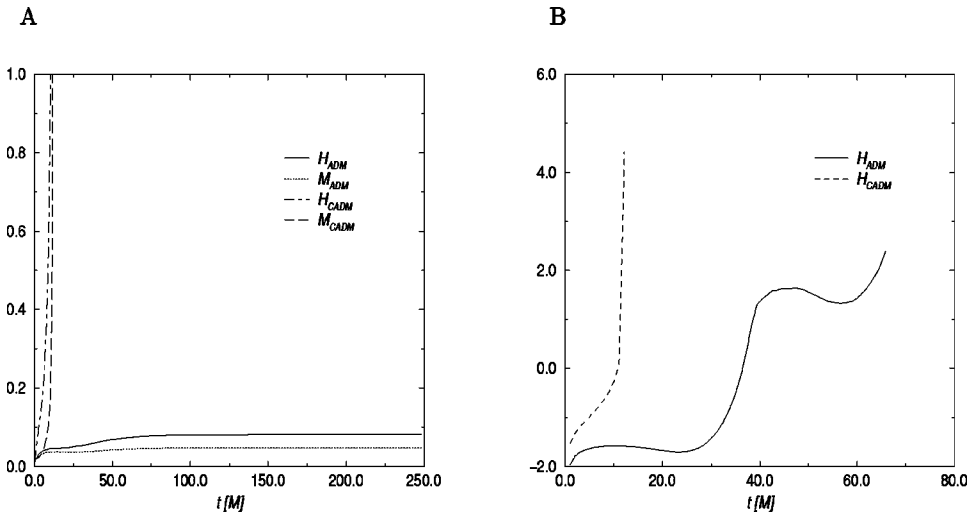

FIG. 2. The L_2 norm of the Hamiltonian and momentum constraints vs time for both formulations (discretization size $\Delta r = M/10$) for the case where the domain of integration is $[M,4M]$ (A) and $[M,9M]$ (B). In A, the evolution obtained with the ADM formulation does not show the presence of an exponentially growing mode such as the one obtained with the CADM approach. However, for the larger domain (B), solutions obtained with both formulations are exponentially growing.

of this exponential mode will likely spoil any long term simulation. For the CADM system, irrespective of the value of n exponential modes are clearly present in the solutions.

These results are illustrated in Fig. 2, which shows the L_2 norm of the Hamiltonian and momentum constraints of the solutions obtained with both formulations when $n=4$. Clearly, the solution obtained with the ADM is better than that obtained with the CADM. Figure 2 also displays the L_2 norm of the Hamiltonian constraint for the case $n=9$, although the solution obtained with the ADM formulation can be considered better than that from the CADM, both grow exponentially.

2. Locked evolution

It has been observed in the literature [12] that in the case where K is fixed in time very long term evolutions can be obtained with the CADM system. Keeping K fixed in time can be achieved by either choosing to not evolve Eq. (2.6c) (what we call ''*forced locking*''), as is done in Ref. [12] or by judiciously taking advantage of the gauge freedom (what we call *dynamical locking*). We next examine both possibilities.

Forced-locking. In this case, we fix the value of $K(t,r)=K(t=0,r)$ throughout the evolution. Note that under this choice, ϕ also remains unchanged in the present case (since β and K are then fixed to their analytic values). Therefore the determinant of the three metric γ_{ij} will remain independent of time. This could be regarded as an evolution that ''locks'' the volume which bears some similarity with the so-called ''area-locking'' gauge [18,26]. Under this condition, stable evolutions can be obtained with $n \lesssim 16$. For $n \gtrsim 16$ long term evolutions ($\gtrsim 100M$) display at late times a clear exponentially growing mode.

A somehow related strategy can be implemented in the ADM case as it has been shown in Ref. [26]. In this work, one chooses not to evolve Eq. (2.1a) for $i=j=\theta$ and stable evolutions are obtained in domains with $n \lesssim 11$. For $n \gtrsim 11$ instabilities appear at considerable later times ($\gtrsim 100M$) than the case where $\gamma_{\theta\theta}$ is not fixed in time.

Figure 3 shows the L_2 norm of the Hamiltonian and momentum constraints corresponding to solutions obtained with both formulations for the choice $n=4$ and $n=9$. In both cases the simulations can be performed for unlimited time without observing exponential modes. Again, the solution obtained with the ADM formulation is slightly more accurate than that provided by the CADM formulation.

As an aside, let us comment on an additional observation in [12] on the behavior of the $\tilde{\gamma}^{ij}\tilde{A}_{ij}$. Although $\tilde{A}_{ij}$ is defined to be trace-free, the numerical evolution does not necessarily preserve such condition and the trace drifts away from zero. By controlling this drift (by appropriately subtracting the trace at each time step) better behaved evolutions are obtained by Alcubierre *et al.* in Ref. [12]. In our present work, we indeed observe such a drift but it remains under control unless the evolution becomes unstable. We also tried subtracting the trace as proposed in Ref. [12] but its implementation did not significantly change the outcome. This may be explained by the fact that our studies have been carried out in a spherically symmetric setting (1D) while those in Ref. [12] have been carried out in 3D (without black hole excision).

Dynamical-locking. The results from the previous section are certainly encouraging as the forced locking of K (for the CADM formulation) or $\gamma_{\theta\theta}$ (for the ADM system) enable much longer evolutions. However, choosing to do so is unphysical in generic situations. One would like to have a prescription where a similar condition can be enforced without having to not evolve one or more equations. For the ADM system, several suggestions have been made to maintain either $\gamma_{\theta\theta}$ or the determinant of the angular part of γ_{ij} fixed via a careful choice of coordinate conditions [18,15,26]. For the CADM system one can also use the coordinate freedom to demand that $\partial_t K=0$. For instance, the use of a maximal

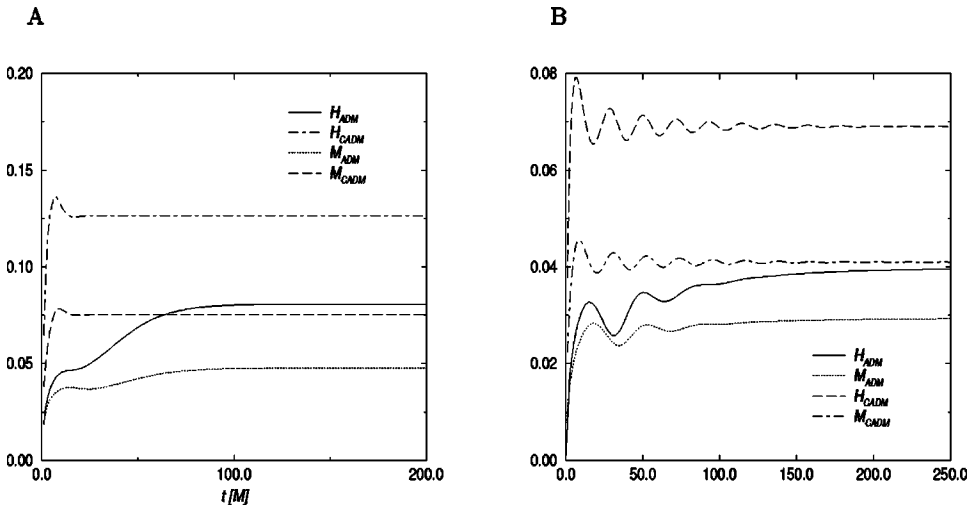

FIG. 3. The L_2 norm of the Hamiltonian and momentum constraints vs time for both formulations (with $\Delta r = M/10$) for the case where the domain of integration is $[M,4M]$ (A). Neither formulation displays exponential modes in this domain and the ADM one yields more accurate results. In (B), the L_2 norm of the Hamiltonian and momentum constraints of the solution obtained with the CADM and an ''area-locked'' ADM evolution (in the $[M,9M]$ domain) is shown, a transient oscillatory behavior is present at earlier stages and the solutions then settle to a constant value.

slicing of the spacetime [29] i.e., $K=0$ will trivially satisfy this condition. However, in practical numerical applications $K\equiv 0$ might not be the most convenient slicing choice [30] (for instance, the Schwarzschild spacetime in Eddington-Finkelstein coordinates does not have $K=0$); thus, one would like to avoid such a strong requirement while still controlling the evolution of K.

A practical way of choosing such a coordinate condition is to define the shift vector from Eq. (3.2c),

$$\beta^i \partial_i K = \gamma^{ij} D_i D_j \alpha - \alpha \left[\tilde{A}_{ij} \tilde{A}^{ij} + \frac{1}{3} K^2 \right], \qquad (4.6)$$

which clearly keeps $\partial_t K = 0$ but allows K to vary in space. This condition is straightforward to implement in 1D but is certainly more complicated in 3D. Additionally, there is a great deal of ambiguity as it is only one equation for three variables β^i. Therefore two supplementary conditions must be chosen so that Eq. (4.6) can be used to ''freeze'' the evolution of K. In our present implementation we have simply chosen $\beta^A = 0$ [with $A=(\theta,\phi)$] and obtained β^r with Eq. (4.6) as

$$\beta^r = \frac{1}{\partial_r K} \left(\gamma^{ij} D_i D_j \alpha - \alpha \left[\tilde{A}_{ij} \tilde{A}^{ij} + \frac{1}{3} K^2 \right] \right). \qquad (4.7)$$

A straightforward way to obtain β^r is by a first order approximation of the right-hand side of Eq. 4.7 (i.e., evaluating each term at the old level). By using this condition, instead of choosing not to evolve K, we were able to obtain evolutions not displaying exponential modes for times larger than $250M$ (with resolutions of $\Delta r = M/10$ and finer). Figure 4 illustrates what is obtained in a simulation with computational domain defined by $[M,11M]$ (with $\Delta r = M/10$). The values of the L_2 norms of the Hamiltonian, the function $F - F_{t=0}$ and value of $K - K_{t=0}$ are shown as a function of time. Since β^r is obtained only as a first order approximation, K and F are expected to vary during the evolution. As can be seen in Fig. 4, both grow linearly but stay fairly close to zero and the evolution proceeds without displaying an exponential growth.

3. Perturbed evolution

In this case, we test the evolutions under perturbations (using a locked evolution in the CADM case but not in the ADM one). The initial data corresponds to the analytic value of γ_{rr} (or $\tilde{\gamma}_{rr}$) plus some arbitrary pulse of compact support. Of course, this data is unphysical but we use it to probe for stability of the implementations in a nontrivial scenario. The

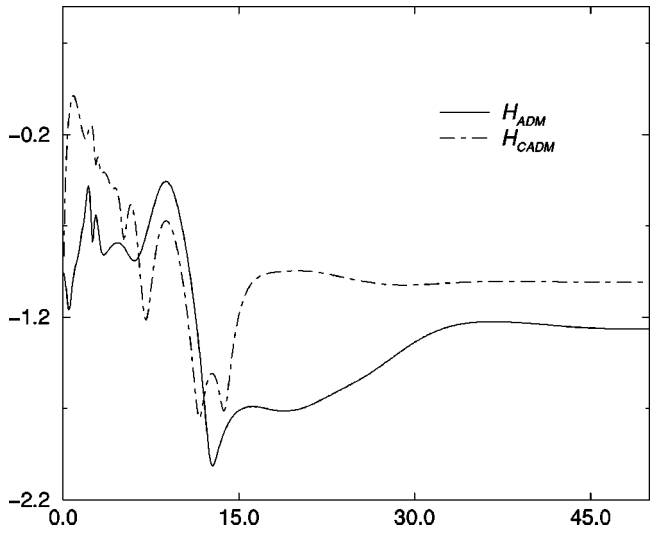

FIG. 4. The L_2 norms of the Hamiltonian constraint and the differences $F - F_{t=0}$ and $K - K_{t=0}$ vs time. The evolution proceeds without displaying exponential modes and the value of $||K - K_{t=0}||_2$ stays close to zero.

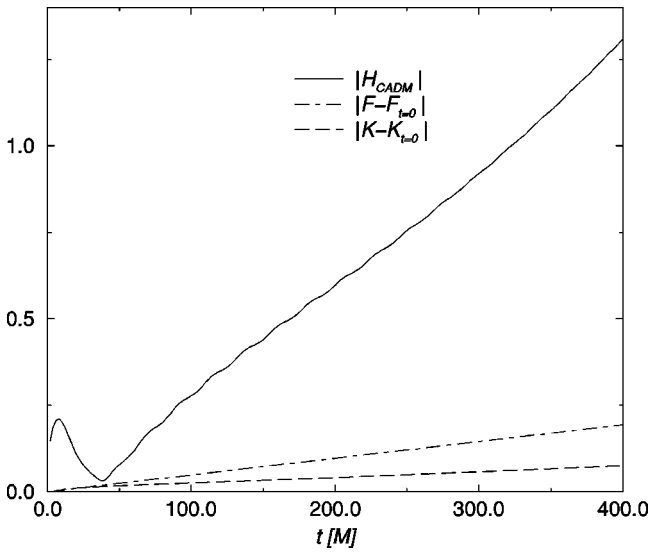

FIG. 5. The L_2 norm of the Hamiltonian constraint vs time for the perturbed evolutions (where K has been frozen in the CADM evolution while all fields are evolved in the ADM one, with computational domain in $[M,6M]$). After some initial transient behavior both settle into an stationary solution.

amplitude of the pulse is chosen such that it can be considered a linear perturbation of a Schwarzschild spacetime. The results obtained with both codes agree with those of the previous section. Figure 5 corresponds to the evolution of a pulse with compact support in $[3M,5M]$ being evolved in a computational domain of $[M,6M]$. The L_2 norm of the Hamiltonian constraint, after some initial transient behavior, settles into a stationary regime.

B. Causal differencing and domain of dependencies

As a last point, it is interesting to see how causal differencing is indeed providing a correct way to discretize the equations taking advantage of the causal properties of the spacetime. The fact that the null cones (or the causal domain of dependence) are tilted inside the horizon, allows for a stable numerical implementation where inner boundary data need not be provided if the inner boundary is inside the black hole (see Fig. 6). This is possible because the numerical domain of dependence naturally contains the causal domain of dependence of the inner boundary point. The condition of the numerical domain of dependence containing the causal domain of dependence is a necessary condition for stability and is known as the Courant-Friedrichs-Levy (CFL) condition [28].

This condition cannot be fulfilled if the innermost point is outside the event horizon. In order to illustrate this fact we compare two cases where the innermost point is placed inside or just outside the event horizon and use the ADM system to obtain the solution. As illustrated in Fig. 7, while the solution obtained with the inner boundary inside the black hole is stable, the other, as expected is unstable.

V. CONCLUSIONS

The results presented in this work show that excision techniques can be straightforwardly used in the CADM formulation directly from the structures developed for the ADM formulation. The ADM formulation is superior to the CADM both in accuracy and total time evolution when the evolution of K is not locked in CADM. When locking is implemented, then CADM is better than ADM as the solution obtained with the CADM formulation does not display exponential modes with the outer boundary placed as far as $16M$. On the other hand, evolutions with the ADM formulation display exponential modes with the outer boundary placed at $11M$ and beyond. Additionally, for the case where outer boundaries are placed ''very'' far, although exponentially growing solutions are present in solutions obtained with both formulations, ADM simulations crash at earlier times than those obtained with the CADM system.

It is worth remarking again that in both formulations, implementing a gauge that minimizes the changes in some of

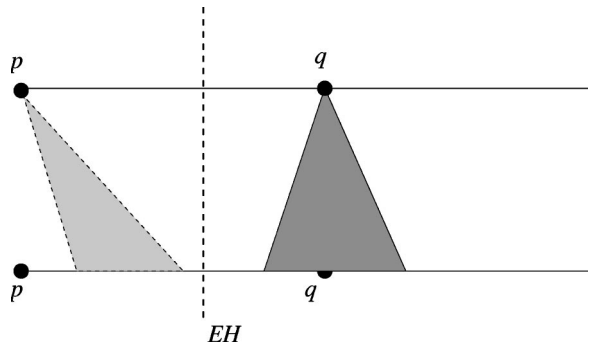

FIG. 6. Domains of dependence of points inside and outside the event horizon (EH). Inside the EH, the past null cone of p is tilted, therefore the evolution algorithm does not need the value of the fields at p on the old level.

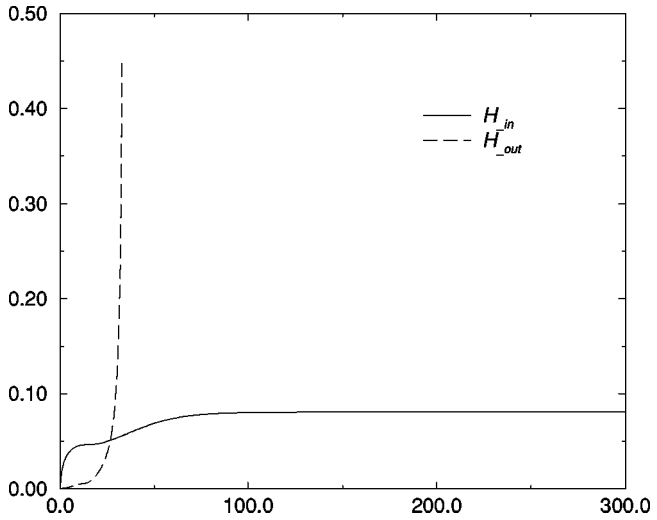

FIG. 7. The L_2 norm of the Hamiltonian constraint vs time for the cases where the inner boundary is inside (at $r=1.5M$ denoted with a solid line) and outside (at $r=2.2M$ denoted with a dashed line) the event horizon (using the ADM formulation). Since the latter does not respect the CFL condition, the obtained solution is unstable. (The values shown correspond to a discretization of size $\Delta r=M/10$ and no qualitative difference is observed with finer resolutions.)

the fields (like $\gamma_{\theta\theta}$ in the ADM formulation or K in the CADM one) dramatically improves the evolutions in 1D. In the 3D case, the use of ''area or circumference locking''[3] is indeed more complicated than locking K, simply by the fact that in the former case one is trying to control a tensor component while in the latter a scalar. Thus, locking K is likely to have an easier and probably more general implementation than area locking (although in cases where the final black hole is close to a nonspinning one, this implementation is rather straightforward). Controlling the evolution of K demands a condition such as that given by Eq. (4.6), and two extra conditions on β^i will be required. An option that mimics the 1D implementation is to foliate the 3D hypersurfaces with a sequence of two-surfaces defined by $\Theta = \text{const}$ (with Θ the expansion of outgoing null rays). Once this foliation is obtained, the shift vector β^i could be decomposed as

$$\beta^i = \beta^i_{|} + \beta^i_{\perp} \tag{5.1}$$

with $\beta^i_{|}$ ($\beta^i_{\perp}$) parallel (perpendicular) to the normal of the two-surfaces. Thus, the two further conditions can be chosen such that $\beta^i_{\perp} = \text{const}$, thus minimizing changes in transversal directions. Of course, this is just one possible approach and further studies will be required to obtain a K fixing condition that leads to a practical implementation.

In conclusion, implementing singularity excision via causal differencing techniques in the CADM formulation is straightforward. Its usefulness depends on enforcing a gauge controlling the behavior of K. Assuming this can be achieved, CADM appears to be capable of providing more robust simulations than ADM when the outer boundary is placed farther than $11M$ from the final black hole of mass M, if the outer boundary is closer, then the ADM formulation provides evolutions as stable as the CADM one but with better accuracy.

Lastly we would like to add two remarks. First, we want to stress that we have only applied the causal differencing algorithm described in Refs. [22,21] since at present is the only one fully implemented in $3D$. Other alternatives have been proposed [19,20,31]; due to the restriction to spherical symmetry it is likely that the application of these will yield similar results to those presented in this work. Second, our present work has compared the use of causal differencing in two formulations of Einstein field equations. Although causal differencing has been the method that has so far received the most attention, other techniques are being explored in 3D. For instance, in Ref. [32] the use of up-wind type algorithms has been shown to be a viable alternative when the resolution is about $M/40$ or finer. To present implementations this resolution is fairly costly; however, techniques such as adaptive mesh refinement, domain decomposition, etc., should allow researchers to explore and implement a wider range of options.

[3]i.e., controlling the determinant of the angular part of the metric (area locking) or $g_{\theta\theta}$ (circumference locking).

ACKNOWLEDGMENTS

This work was supported by NSF PHY 9800725 to the University of Texas at Austin and NSF 9800970 and NSF 9800973 to the Pennsylvania State University. We thank D. Neilsen, P. Marronetti, R. Matzner, P. Laguna, and J. Pullin for helpful comments and suggestions. D.G. thanks the Alfred P. Sloan Foundation for support.

APPENDIX: STABILITY ANALYSIS OF THE INTERPOLATION PHASE

As described in Sec. III, the evolution is carried over in two steps. The first one (A), provides field values at the new level while the second (B) interpolates these values to obtain the fields at grid points. It is important to notice that a ''stable'' implementation of the first step (A) does not guarantee that the overall integration algorithm (steps A+B) will be stable. This fact unfortunately appears to have been overlooked in the literature. We find thus important to remark which options for B will not spoil the overall stability of the evolution algorithm. Our analysis will be *independent* on how step A is performed; rather, we will assume that we have a solution at the new level and concentrate on which interpolation stencil will yield a procedure that does not spoil the scheme's overall stability. We proceed by performing a straightforward von Neumann stability analysis. We start by assuming that the solution u at the new level can be decomposed in eigenmodes of the form

$$u^n_j = \xi^n e^{ikj\Delta r}. \tag{A1}$$

Then, we obtain the value of u at the point of interest r_j by an interpolation, i.e.,

$$u^n(r_j) = \sum_{s=j-l}^{j+r} u^n_s W(r, r_s), \tag{A2}$$

where $j-l$ and $j+r$ define the left and right limits of the interpolating stencil and $W(r,r_s)$ denotes the weight of u^n_j in the interpolating procedure. Replacing Eq. (A1) in Eq. (A2),

$$u^n(r_j) = u^n_j \sum_{s=-l}^{r} e^{iks\Delta r} W(r, r_{j+s}). \tag{A3}$$

Let us assume that step A has been carried in a stable manner, hence $|u^n_j| \leqslant 1$. A necessary condition for the combination of steps A and B to be stable is

$$|S| \equiv \left| \sum_{s=-l}^{r} e^{iks\Delta r} W(r, r_{j+s}) \right| \leqslant 1, \tag{A4}$$

which depends solely on the interpolation stencil. We next show what the results are for a choice of second, third and fourth order accurate stencils obtained using a Lagrangian interpolating polynomial.

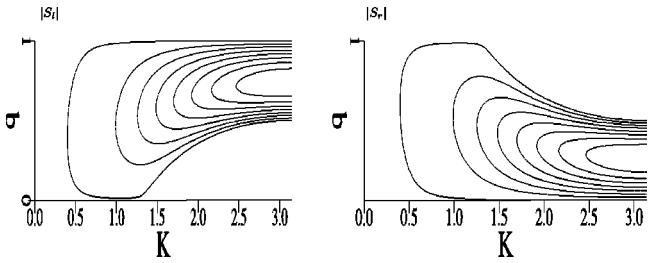

FIG. 8. Contour plots corresponding to the amplification factors for S_l and S_r as a function of b and $K \equiv k\Delta r$. The contours display the region where the amplification results larger than 1. In both cases, the outermost curve corresponds to a value of 1.001 and determines a region whose interior has amplification larger than 1. The sequence of curves correspond to values given by $1.001 + 0.027s$ $(s=0-7)$.

1. Second order

Assuming the point we are interested in is at $r=r_j + b\Delta r$, with $b \in (0,1)$. The interpolating polynomial involves values at r_j and r_{j+1}; after a straightforward evaluation,

$$|S| = \sqrt{1+2b(b-1)[1-\cos(k\Delta r)]}. \tag{A5}$$

Clearly, $|S| \leqslant 1 \forall b \in (0,1)$, thus a second order accurate interpolation cannot, by itself, render the evolution unstable.

2. Third order

Again, we assume the location of interest is $r=r_j+b\Delta r$ [with $b \in (0,1)$]. In this case, one has two options to obtain a third order accurate value by either using the points r_{j-1} through r_{j+1} or r_j through r_{j+2} in the interpolating stencil. We denote the values of S with either S_l for the former case and S_r for the latter. After rearranging terms one obtains

$$|S_l| = \sqrt{1+b(b-2)(b-1)^2(\cos(k\Delta r)-1)^2}, \tag{A6}$$

$$|S_r| = \sqrt{1+b^2(b^2-1)(\cos(k\Delta r)-1)^2}. \tag{A7}$$

From these, $|S_r| \leqslant 1$ and $|S_l| \leqslant 1 \forall b \in (0,1)$. As in the second order case, the interpolation cannot render the whole integration unstable.

3. Fourth order

In this case, we have three stencil options: left-sided, when using r_{j-2} through r_{j+1}; centered, when using r_{j-1} through r_{j+2}; and right-sided, when using r_j through r_{j+3}. We denote the amplification factors for these three cases with S_l, S_c, and S_r, respectively. The expressions for them are rather lengthy and analyzing their values is not as direct as in the previous cases. It turns out to be more convenient to simply plot their values as a function of both b and $K \equiv k\Delta r$ (for all possible values of b and K). Figure 8 displays the regions where S_l and S_r have values be larger than 1 (the centered scheme has $|S_c| \leqslant 1$ and we do not include it in the contour plot figures). As can be seen in Fig. 8, the interpolation procedure can induce instabilities for $b \in (0,1)$ even for low frequency modes. Thus, unless the point under consideration lies at the center cell of the stencil, a fourth order interpolation scheme, can by itself render the whole evolution scheme unstable.

[1] M. Huq, in Proceedings of the BBH Grand Challenge Meeting, Pittsburgh, Pennsylvania, 1997 (unpublished).

[2] G. Gook and M. Scheel, in Proceedings of the BBH Grand Challenge Meeting, Austin, Texas, 1998 (unpublished).

[3] J. Thornburg, Class. Quantum Grav. **14**, 1119 (1987).

[4] For instance, H. Friedrich, Proc. R. Soc. London **A375**, 169 (1981); S. Frittelli and O. Reula, Phys. Rev. Lett. **76**, 4667 (1996); A. Anderson and J. York, *ibid.* **82**, 4384 (1999). [For a detailed list of hyperbolic formulations see O. Reula, ''Hyperbolic Methods for Einstein's equations,'' Living Reviews (1998).]

[5] C. Bona, J. Masso, E. Seidel, and J. Stela, Phys. Rev. D **56**, 3405 (1997).

[6] M. Shibata and T. Nakamura, Phys. Rev. D **52**, 5428 (1995).

[7] T. Baumgarte and S. Shapiro, Phys. Rev. D **59**, 024007 (1999).

[8] S. Frittelli and O. Reula, J. Math. Phys. **40**, 5143 (1999).

[9] L. L. Smarr and J. W. York, Phys. Rev. D **17**, 2529 (1978); P. R. Brady, J. D. Creighton, and K. S. Thorne, *ibid.* **58**, 061501 (1998); C. Gundlach and D. Garfinkle, Class. Quantum Grav. **16**, 4111 (1999).

[10] For a recent review see J. Font, ''Numerical Hydrodynamics in General Relativity,'' Living Reviews (2000).

[11] K. Oohara and T. Nakamura, Prog. Theor. Phys. Suppl. **136**, 270 (1999).

[12] M. Alcubierre, G. Allen, B. Brügmann, T. Dramlitsch, J. Font, P. Papadopoulos, E. Seidel, N. Stergioulas, W. M. Suen, and R. Takahashi, Phys. Rev. D **62**, 044034 (2000).

[13] B. Brügmann, Int. J. Mod. Phys. D **8**, 85 (1999).

[14] The Binary Black Hole Grand Challenge Alliance, Phys. Rev. Lett. **80**, 2512 (1998).

[15] R. Marsa and M. Choptuik, Phys. Rev. D **54**, 4929 (1996).

[16] C. Misner, K. S. Thorne, and J. Wheeler, *Gravitation* (Freeman, San Francisco, 1973).

[17] M. Alcubierre, G. Allen, B. Buegman, E. Seidel, and W. M. Suen, ''Towards an understanding of the stability properties of the 3+1 evolution equations in general relativity,'' gr-qc/9908079, 1999.

[18] E. Seidel and W. M. Suen, Phys. Rev. Lett. **69**, 1845 (1992).

[19] M. Alcubierre and B. Schutz, J. Comput. Phys. **112**, 44 (1994).

[20] C. Gundlach and P. Walker, Class. Quantum Grav. **16**, 991 (1999).

[21] M. Scheel, T. Baumgarte, G. Cook, S. Shapiro, and S. Teukolsky, Phys. Rev. D **56**, 6320 (1997).

[22] M. Huq and R. Matzner (unpublished).

[23] URL http://www.astro.psu.edu/users/nr/Agave/

[24] S. Teukolsky, Phys. Rev. D **61**, 087501 (2000).

[25] A. E. Eddington, Nature (London) **113**, 192 (1924); D. Finkelstein, Phys. Rev. **110**, 965 (1958).

[26] L. Lehner, M. Huq, M. Anderson, E. Bonning, D. Schaefer, and R. Matzner, Phys. Rev. D **62**, 044037 (2000).
[27] R. Gomez, in Proceedings of the BBH Grand Challenge Meeting, Los Alamos, New Mexico, 1997.
[28] B. Gustaffson, H. Kreiss, and J. Oliger, *Time Dependent Problems and Difference Methods* (Wiley, New York, 1995).
[29] A. Lichnerowicz, J. Math. Pures Appl. **23**, 37 (1944).
[30] J. W. York, in *Sources of Gravitational Radiation*, edited by L. Smarr (Cambridge University Press, Cambridge, England, 1979).
[31] R. Gomez, L. Lehner, R. Marsa, and J. Winicour, Phys. Rev. D **57**, 4778 (1998).
[32] J. Thornburg, ''A 3+1 Computational Scheme for Dynamic Spherically Symmetric Black Hole Spacetimes II: Time Evolution,'' gr-qc/9906022, 1999.